Combined EXAFS and Powder Diffraction Analysis

N. Binsted, M. J. Pack, M. T. Weller,* and J. Evans

Contribution from the Department of Chemistry, University of Southampton, Southampton SO17 IBJ, UK

Received September 22, 1995. Revised Manuscript Received May 7, 1996[⊗]

Abstract: A method has been developed which allows the simultaneous refinement of X-ray powder diffraction data and one or more EXAFS spectra from the same sample using a single set of coordinates to describe the structure. The atomic positions are refined together with isotropic thermal factors, peak shape and amplitude parameters, and the EXAFS energy zeros for each absorption edge. The program determines the point symmetry and radial coordinates of each site occupied by an atom for which EXAFS data are available, allowing a full multiple scattering calculation to be performed for each site. Mixed or partial occupancy of sites is permitted. Where correlations between atoms can be calculated, as with copper for which Debye theory can be used, EXAFS mean-square displacements can be derived from the isotropic thermal factors, otherwise either the correlations or the EXAFS mean-square relative displacements must be introduced as separate variables. The method potentially allows us to accurately determine the position of oxygen and other light atoms in materials where the diffraction pattern is dominated by heavy atoms, and to determine the occupancy of sites where elements of similar scattering amplitude are involved. Results are particularly good where the EXAFS of several absorbing atoms are available.

Introduction

The techniques of extended X-ray absorption fine structure (EXAFS) and X-ray powder diffraction (XRD) have often been combined in the study of materials. In most cases this is due to the complementarity of the methods rather than a simply confirmatory role. One aspect often utilized is that the short-range order seen by EXAFS contrasts with the long-range order seen by XRD. This has been used in real time QUEXAFS studies of the crystallization of amorphous materials and other solid-state reactions.[1,2]

However, even with well-ordered crystalline materials there are differences in the information available from the two techniques. The atom specific nature of EXAFS allows the determination of minor or trace elements within the structure.[3,4] In this situation EXAFS measurements may be made after the bulk properties, such as site coordinates and cell parameters, have been established by powder diffraction studies. EXAFS may then reveal the site occupancies of minor components. Another EXAFS application of considerable importance is the determination of the positional coordinates of major elements within crystalline materials where certain site coordinates or occupancies are not well resolved by XRD alone. Cases where this may occur include the following: (a) sites occupied by light atoms when the diffraction pattern is dominated by heavy atom contributions, (b) when the contributions of the scattering from two different crystallographic sites are exactly equivalent in terms of their contributions to overlapping reflections in the powder pattern, (c) when different sites are occupied by atoms of only slightly different atomic number, and (d) when sites are partially occupied by different atom types. In such cases EXAFS may provide significant additional information allowing a unique determination of the structure where ambiguities occur in the XRD determined structure.

Previously Currie et al.[5] have used EXAFS data to resolve the identity of iodine and group IV element (M′) sites in mixed metal periodates using EXAFS spectra associated with both edges. This analysis provides accurate individual M′−O and I−O distances, but determination of accurate positional parameters for the iodine and the group IV element sites was not possible, and the marked discrepancy in the EXAFS and XRD distances remained unresolved. The solution, presented here, is to refine both the XRD and EXAFS spectra simultaneously. This has a number of additional advantages. One advantage is that no additional structural variable needs to be introduced in order to describe the EXAFS distances, even when very many shells are fitted, thus the method is a far more rigorous test of a structural model than either of the techniques performed independently and should lead to a better determined refinement. The assessment of errors in a combined refinement is also, in principal, easier than when two separate refinements are made. The idea of combining information from other techniques with XRD data has been applied to combined X-ray and neutron diffraction analysis.[6,7] The technique of diffraction anomalous fine structure (DAFS)[8] exploits aspects of the combined XRD/EXAFS method. A preliminary description of an earlier version of this program has previously been published.[9]

Experimental Section

EXAFS spectra were measured at Daresbury Laboratory's Synchrotron Radiation Source. Spectra were recorded in transmission mode using monochromatic radiation obtained using harmonic-rejecting double-crystal monochromators (Si(111) or Si(220)). Measurements

[⊗] Abstract published in *Advance ACS Abstracts,* October 1, 1996.

(1) Dent, A. J.; Greaves, G. N.; Couves, J. W.; Thomas, J. M. *Synchrotron Radiat. Dyn. Phenom.* **1991**, 631.

(2) Sankar, G.; Wright, P. A.; Natarajan, S.; Thomas, J. M.; Greaves, G. N.; Dent, A. J.; Dobson, B.; Ramsdale, C. A.; Jones, R. H. *J. Phys. Chem.* **1993**, *97*, 9550.

(3) Battle, P. D.; Catlow, C. R. A.; Chadwick, A. V.; Greaves, G. N.; Moroney, L. M. *J. Phys.* **1986**, *C8*, 669.

(4) Charnock, J. M.; Garner, C. D.; Patrick, R. A. D.; Vaughan, D. J. *J. Solid State Chem.* **1989**, *82*, 279.

(5) Currie, D. B.; Levason, W.; Oldroyd, R. D.; Weller, M. T. *J. Mater. Chem.* **1993**, *3*, 447. Currie, D. B.; Levason, W.; Oldroyd, R. D.; Weller, M. T. *J. Mater. Chem.* **1994**, *4*, 1.

(6) Crennell, S. J.; Owen, J. J.; Clare, P. G.; Cheetham, A. K.; Kaduk, J. A.; Jarman, R. H. *J. Mater. Chem.* **1991**, *1*, 113.

(7) GSAS; Larsen, A. L.; von Dreele, R. B. MS-H805, Los Alamos National Laboratory.

(8) Pickering, I. J.; Sansone, M.; Marsch, J.; George, G. N. *J. Am. Chem. Soc.* **1993**, *115*, 6302. Pickering, J. J.; Sansone, M.; Marsch, J.; George, G. N. *Jpn. J. Appl. Phys.* **1993**, *32−2*, 206.

(9) Binsted, N.; Weller, M. T.; Evans, J. *Phys. B* **1994**, *208 and 209*, 129.

S0002-7863(95)03251-3 CCC: $12.00

were on powdered samples mixed with boron nitride, at room temperature. Data used in this work generally derived from two or three scans over a limited *k*-range except for copper and copper oxide where a single good-quality scan was sufficient. These data do not represent the ultimate data quality that the technique can achieve but are typical of the quality of spectra normally obtained. XRD measurements were also made at room temperature using a Siemens D5000 diffractometer operating with copper $K\alpha_1$ radiation; data were typically collected over a period of 15 h with a step size of 0.02°. No external calibration was used. For optimum results samples could be cooled to liquid nitrogen temperatures for both sets of measurements. EXAFS data were background subtracted using the program PAXAS.[10] The pre-edge background was approximated by a quadratic function, and the atomic contribution (μ_0) above the edge by coupled polynomials allowing the EXAFS contribution χ to be extracted from the pre-edge subtracted absorbance (μ) according to

$$\chi(E) = \frac{(\mu(E) - \mu_0(E))}{\mu_0(E)} \tag{1}$$

where E is the photon energy with respect to an arbitrary origin, taken here as the maximum in $d\mu/dE$. In a few cases monochromator glitches were removed during background subtraction, but otherwise spectra fitted were raw data and no smoothing or Fourier filtering was employed.

Theory. The EXAFS method used is based on the fast spherical wave formalism of Gurman, Binsted, and Ross.[11,12] Multiple scattering to the fifth order is included but in most cases only third-order scattering involving no more than two scattering atoms is used. Ground-state photoelectron potentials are calculated according to the Mattheis prescription.[13−15] Excited-state corrections to the exchange and correlation potential are based on the theory of Hedin and Lundquist[16] as implemented by Lee and Beni.[17] The code used was taken from the program FEFF.[18] The phase shifts are calculated following Fox and Goodwin[19] with modifications to optionally include scalar relativistic terms. The XRD calculations used are based on the DBW code of Wiles, Sakthivel, and Young.[20] Results presented here employ a pseudo-Voigt peak shape and a refinable polynomial background.

When combining the two techniques, it is important to consider any approximations which may give rise to systematic differences between them. In particular systematic errors arise in EXAFS because of the approximations used in calculating the phase shifts, and in the treatment of thermal disorder. Although it is possible to account for differences by introducing additional parameters, such as a scaling factor for EXAFS distances, such terms are undesirable and have been eliminated by improved treatment of disorder and by including, where necessary, one or more of the variables used in phase shift calculations in the refinement. The treatment of disorder is reviewed below. The use of refinable variables in calculating the atomic phase shifts in order to overcome the limitations of the muffin-tin model in complex systems is discussed further elsewhere.[21]

Method

The structural model is first defined as for a Rietveld analysis, in terms of a space group, positional coordinates, and occupancies. For each atom for which EXAFS spectra are available, the program calculates the radial distribution up to a predefined limit (normally 5 to 10 Å). If necessary several clusters will be generated for each structurally unique site occupied by the atom in question. Mixed or partially occupied sites are permitted. For each cluster, the program determines the point group. This allows the table of radial coordinates to be reduced to a set of shell coordinates and occupation numbers, and a point group operator. One benefit is the efficient treatment of multiple scattering (MS) making full use of symmetry without the need for a path-sort to find equivalent paths. It is important to include MS even when it does not make a large contribution to the final result. MS is particularly sensitive to short interatomic distances, and hence its inclusion will help to eliminate solutions where distances are significantly shorter than actual values. The XRD and EXAFS theories may then be calculated. Least-squares refinement during the combined EXAFS and XRD curve fitting involves minimization of the weighted sum of squares of residuals employing the nonlinear least-squares routine VA05A in the Harwell library.[22]

In addition to the structural parameters required to describe the model, the parameters refined are the XRD isotropic thermal parameters, peak shape and background parameters, scale factor, and zero offset. When EXAFS Debye−Waller factors A ($= 2\sigma^2$) are refined, the first few strongly correlated values are treated separately except for closely spaced shells, while for remote shells all atoms of similar Z are treated similarly. The EXAFS energy zero EF (one per spectrum) and optionally one or more phase shift parameters are also refined. Examples of phase shift parameters include a common interstitial potential term (V_0) or individual muffin-tin radii.

The program also allows restraints for molecular groups or interatomic distances and angles to be applied,[23] which are often very helpful in finding an initial solution. In addition, constraints due to occupation of special positions (e.g. *x*,*x*,*x*) can be defined. Most of the other features available with the EXCURVE package such as generation of contour maps of the fit-index due to pairs of variables, statistical analysis, and generation of formatted tables of refined variables are also available.

The quantity minimized during refinement is given by:

$$W_{\text{exafs}}\phi_{\text{exafs}} + W_{\text{xrd}}\phi_{\text{xrd}} \tag{2}$$

W_{exafs} and W_{xrd} are the weights attached to the EXAFS and XRD data sets, respectively. Additional terms are added if constraints are used.

The EXAFS contribution is given by:

$$\phi_{\text{exafs}} = \sum_i^N w_i(\chi_i^{\text{exp}}(k) - \chi_i^{\text{th}}(k))^2 \tag{3}$$

$\chi^{\text{exp}}(k)$ and $\chi^{\text{th}}(k)$ are the experimental and theoretical EXAFS. k is the magnitude of the photoelectron wavevector. w_i, the weighting attached to a particular data point i, is normally defined for an EXAFS data point by:

$$w_i^{1/2} = \frac{k_i^n}{\sum_j^N k_j^n |\chi_j^{\text{exp}}(k)|} \tag{4}$$

(10) Binsted, N. PAXAS; EXAFS analysis program, 1988.
(11) Gurman, S. J.; Binsted, N.; Ross, I. *J. Phys. C* **1984**, *17*, 143.
(12) Gurman, S. J.; Binsted, N.; Ross, I. *J. Phys. C* **1986**, *19*, 1845.
(13) Mattheis, L. F. *Phys. Rev. B* **1973**, *8*, 3719.
(14) Loucks, T. L. *Augmented Plane Wave Method*; W. A. Benjamin: New York, 1967; p 1.
(15) Binsted, N.; Norman, D. *Phys. Rev. B* **1994**, *49*, 15531.
(16) Hedin, L.; Lundquist, S. *Solid State Phys.* **1969**, *23*, 1.
(17) Lee, P. A.; Beni, G. *Phys. Rev. B* **1977**, *15*, 2862.
(18) Rehr, J. J.; Albers, R. C.; Zabinsky, S. I. *Phys. Rev. Lett.* **1992**, *69*, 3397. Rehr, J. J.; Mustre de Leon, J.; Zabinsky, S. I.; Albers, R. C. *J. Am. Chem. Soc.* **1991**, *113*, 5135.
(19) Fox, L.; Goodwin, E. T. *Trans. Cambridge Philos. Soc.* **1949**, *45*, 373.
(20) Wiles, D. B.; Sakthivel, A.; Young, R. A. Georgia Institute of Technology, 1991.
(21) Binsted, N.; Hasnain, S. S. *J. Synchrotron Radiat.* Accepted for publication.
(22) AERE Harwell, 1987, Harwell Subroutine Library: a catalogue of subroutines; Harwell Report AERE R 9185 (HMSO), pp 1−72.
(23) Binsted, N.; Strange, R. W.; Hasnain, S. S. *Biochemistry* **1992**, *31*, 12117.

where n is selected to give an envelope of approximately constant amplitude for $k^n\chi^{exp}(k)$.

Similarly the XRD contribution is given by:

$$\phi_{xrd} = \sum_i^N w_i(y_i^{exp} - y_i^{th})^2 \quad (5)$$

where the sum is again over all experimental data points i with experimental and theoretical counts y^{exp} and y^{th}, respectively. For an XRD observation we take the point weighting to be $w_i = 1/y_i^{exp}$.

An R factor is defined as:

$$R_{exafs} = \sum_i^N 1/\sigma_i(|\chi_i^{exp}(k) - \chi_i^{th}(k)|) \times 100\% \quad (6)$$

which gives a meaningful indication of the quality of fit to the EXAFS data in k-space.

A value of around 20% would normally be considered a reasonable fit, with values of 10% or less being difficult to obtain on unfiltered data. Similar expressions widely used to assess XRD data[24] are:

$$R_{wp} = \left(\frac{\sum_i w_i(y_i^{exp} - y_i^{th})^2}{\sum_i w_i(y_i^{exp})^2}\right)^{1/2} \times 100\% \quad (7)$$

and, using derived reflection intensities I_i

$$R_{Bragg} = \frac{\sum_i |I_i^{exp} - I_i^{th}|}{\sum_j I_j^{exp}} \times 100\% \quad (8)$$

Here the sum is over the number of reflections. R_{wp} is rather dependent on the absolute level of background and the total number of reflections, so although in most cases a fit of 10 to 15% would be acceptable, in others, particularly in systems with very few well-separated reflections, it is impossible to obtain values of less than 30%.

An absolute index of goodness of fit, which takes account of the degree of overdeterminacy in the system, is given by the reduced χ^2 function. For EXAFS this is[25]

$$\epsilon_\nu^2 = 1/(N_{ind} - p)(N_{ind}/N) \sum_i^N w_i(\chi_i^{exp}(k) - \chi_i^{th}(k))^2 \quad (9)$$

where N_{ind} is the number of independent data points and p the number of parameters. N_{ind} is normally less than the number of data points N, and in the case that the data from k_{min} to k_{max} is Fourier filtered using a window r_{min} to r_{max} it is given by:

$$N_i = 2(r_{max} - r_{min})(k_{max} - k_{min})/\pi \quad (10)$$

For XRD the usual procedure[24]

$$S^2 = (R_{wp}/R_{expected})^2 \quad (11)$$

where $R_{expected}$ is

$$R_{expected} = \left(\frac{(N-p)}{\sum_i w_i y_i^2}\right)^{1/2} \times 100\% \quad (12)$$

assumes that each of the N data points contributes to an observation, that is correlation between data points is ignored. This provides a far more generous estimate of the overdeterminacy of a refinement than in the EXAFS analysis. Here, therefore, it is assumed that the number of independent points is given by the number of independent reflections. Although this will be reduced by partial overlaps, the background parameters will indeed depend on the number of data points, producing a reasonable overall result.

The difficulty in comparing the weights for each of the data points w_i for the two techniques, and the fact that it is rarely possible to use experimental values of w_i for EXAFS analysis (accurate distance determination requires a constant amplitude envelope over a wide k-range) complicates the derivation of a useful overall statistical criteria. An expression based on (9) given by

$$\epsilon_\nu^2 = 1/(N_{ind} - p)(N_{ind}/N_{obs}) \sum_i^{N_{obs}} W w_i(f_{exp} - f_{th})^2 \quad (13)$$

is used. The sum is over all observations N_{obs} and where W is W_{exafs}, W_{xrd}, or W_d according to whether the term is due to EXAFS, XRD, or a constraint, respectively. This expression will not have any absolute significance because of the artificial nature of the weightings, but changes will provide a valid statistical measure of the effect of introducing or removing variables—introducing an additional variable should result in an overall reduction in ϵ_ν^2.

Treatment of Disorder. Thermal and static disorder have a significant effect on both XRD and EXAFS spectra, yet in neither technique is disorder treated exactly. The approximations used might be expected to give rise not only to incompatible values for the disorder parameters but also systematic errors in distances. This would mean that two sets of disorder parameters would be required, and errors in distances would give rise to a lack of fit in one or other of the spectra. In order to minimize these problems and attempt to improve upon the previous treatment of disorder in EXAFS[9,11] a more detailed study of the treatment of disorder[26] has been undertaken.

For XRD it is assumed as usual that the thermal disorder associated with each atom can be represented in the harmonic approximation by a mean-square displacement $\langle u^2(\mathbf{r})\rangle$. In general motion is not isotropic with $\langle u^2_x\rangle \neq \langle u^2_y\rangle \neq \langle u^2_z\rangle$. In the examples considered here it is assumed further that motion is isotropic and can be represented by an isotropic thermal factor given by

$$\langle u^2\rangle = B_{isotropic}/(8\pi^2) \quad (14)$$

At present the program does not adequately treat libration corrections or anharmonicity and this issue will be addressed in due course.

An exact treatment of disorder in both techniques requires a configurational average over all possible atomic positions. For EXAFS each path can be treated individually, giving rise to an integral over the three coordinates of each atom in the path.

(24) Young, R. A. *The Rietveld Method*; International Union of Crystallography/Oxford University Press: Oxford, 1993.

(25) Bunker, G. EXAFS Standards Report. *Phys. C* **1990** 999.

(26) Edwards, B.; Tildesley, D. J.; Binsted, N.; Weller, M. T. In preparation.

$$\int\int\int dx_1\, dy_1\, dz_1 \ldots \int\int\int dx_n\, dy_n\, dz_n\, \chi(k,\underline{r_1}\ldots\underline{r_n}) \times g(\underline{r_1}\ldots\underline{r_n}) \quad (15)$$

If many-body correlations are ignored these integrals are of the form

$$\int\int\int dx_1\, dy_1\, dz_1 \ldots \int\int\int dx_n\, dy_n\, dz_n\, \chi(k,\underline{r_1}\ldots\underline{r_n}) \times g_{x_{01}}\ldots \times g_{z_{n0}} \quad (16)$$

Where the g are pair distribution functions for each leg of the scattering path for each coordinate (x,y,z).

For single scattering only, if isotropic motion of each atom is assumed, eq 16 reduces to a single integral over the mean interatomic separation r_m. Due to the effect of motion in three dimensions, r_m differs from the equilibrium separation between atoms r_0 by $r_m = r_0 + \sigma^2/2r_0$ where σ^2, the mean-square separation in interatomic positions, is assumed small in comparison with r_0. This makes the assumption that correlation is isotropic. This integral can be evaluated numerically, avoiding further approximations, or else solved assuming the asymptotic form of the hankel functions, $h(kr) = 1/(kr)e^{ikr}$. An approximate solution in one dimension has been given by Tranquada and Ingalls,[27] which, separating the r-dependent terms in the expression for $\chi(k)$, is:

$$\int_0^\infty dr\, \frac{1}{\sqrt{(2\pi)\sigma}}\, e^{-(r-r_0)^2/2\sigma^2}\, \frac{1}{r^2} \exp^{2ikr} = \frac{1}{r_0^{\,2}} \exp^{2ikr'} e^{-2\sigma^2k^2} \quad (17)$$

where

$$r' = r_0 - 2\sigma^2/r_0 \quad (18)$$

Previously only the Debye−Waller factor $e^{-2\sigma^2k^2}$, neglecting the phase term, has been used. Here there are two options, one to perform the integral numerically, and one to use a plane-wave Debye−Waller factor but including the phase term. All results presented here use the numerical integral which will automatically include spherical wave effects. Failure to include the phase term produces a small but significant apparent shortening in EXAFS distances in most cases. When disorder is large, as in inert gas solids, neglecting this term will give significant errors, such as the apparent thermal contraction noted by a numer of authors.[28] The overall distance correction is however smaller than that of Tranquada and Ingalls,[27] due to the effect of considering motion in three dimensions.

The Debye−Waller term has been generalized to $e^{-1/2\sigma_p^2k^2}$ where σ_p is the mean-square variation in path length. The same expression then describes the amplitude term for multiple scattering paths also. Numerical results indicate that the phase terms are less significant for most MS paths than for single scattering, and for simplicity are neglected. The effects of disorder on bond angles can be represented by calculating the mean bond angle at each atom. This differs significantly from the equilibrium value only for angles close to 180° when disorder will always result in smaller values. MS is particularly sensitive to changes in angles for these values hence the effects can be important and are included.

Third- and fourth-order cumulant terms can now be entered in the program both in the direct integrals and when using the plane-wave Debye−Waller terms. If thermal expansion can be adequately represented by an isotropic coefficient of linear expansion, then only the linear expansion coefficient, α, need be entered in order to calculate the third cumulants for all the shells. This is done using an anharmonic oscillator model.[29] The third cumulant terms appear to make a noticeable contribution to the spectrum and their use in phases such as Cu where the model is good (at least for shells 1, 4, etc.) is being evaluated.

Mean-Square Variation in Path Length. The mean-square variation in path length can be expressed in terms of the atomic mean-square displacements $\langle u_a^2\rangle$, $\langle u_b^2\rangle$, etc. for each atom and the correlations between pairs of atoms C_{ab}. Here anharmonic or anisotropic effects introduced by correlation and many-body correlations are ignored, although they may be important in many cases, and our intention is to include them in further work.

A new expression for the mean-square variation in path length has been derived which takes into account the fact that the photoelectron velocity is fast in comparison with thermal motion. If an atom is included in n legs of the scattering path, the contribution it makes to σ_p is n times of an atom at a "loose end". For σ_p^2 the contribution is n^2 times. This is an important factor leading to a reduction in the contribution of triple scattering paths involving only two or three atoms, such as paths 0-a-0-a-0 or 0-a-b-a-0 (0 is the central atom). For single scattering this generates the traditional term

$$\sigma_p^2 = 4\sigma_{ab}^2 \quad (19)$$

where the mean-square relative displacement σ_{ab}^2 is

$$\sigma_{ab}^2 = (\langle u_a^2\rangle + \langle u_b^2\rangle)(1 - C_{ab}) \quad (20)$$

The general result for σ_p^2 is

$$n_a^2\, \langle u_a^2\rangle\, (1 - Ce_a) \cos^2(\alpha_a/2) + \ldots + n_n^{\,2}\, \langle u_n^{\,2}\rangle (1 - Ce_n) \cos^2(\alpha_n/2) \quad (21)$$

The effective correlations Ce are dependent on all the angles in the path. This can be appreciated by taking a long linear chain of atoms. The correlation affecting an atom at one end is that with the atom at the other end, not any of the atoms in between. If the chain departs from linearity, the intervening atoms will all make some contribution. No accurate solution to this problem has been obtained; it is assumed that all the correlations contribute with a relative weight determined by the same $\cos^2(\alpha/2)$ dependence as in eq 21. Ce is therefore given by:

$$Ce_a = \frac{C_{ab}\cos^2(\alpha_b/2) + C_{ac}\cos^2(\alpha_c/2)\ldots + C_{az}\cos^2(\alpha_z/2)}{\cos^2(\alpha_b/2) + \cos^2(\alpha_c/2)\ldots + \cos^2(\alpha_z/2)} \quad (22)$$

The equation only applies where there is a unique angle at each atom. Complex paths with many non-parallel legs involving the same atom are excluded.

Calculation of Atomic Correlations. In order to obtain meaningful Debye−Waller factors it would be desirable to use just a single isotropic thermal parameter for each site. In order to derive EXAFS Debye−Waller factors, however, it is necessary to calculate the correlations between them as defined by eq 20. The best way to do this is by means of a common theory which will generate both the atomic mean-square displacements, $\langle u^2\rangle$, and the correlations C_{ab}. This can be done using Debye theory. A widely used expression for a monatomic cubic solid

(27) Tranquada, J. M.; Ingalls, R. *Phys. Rev.* **1983**, *B28*, 3520.
(28) Beattie, I. R.; Levason, W.; Binsted, N.; Ogden, J. S.; Spicer, M. D.; Young, N. J. *High Temp. Sci.* **1990**, *26*, 71.
(29) Stern, E. A.; Livins, P.; Zhang, Z. *Phys. Rev. B* **1991**, *43*, 8850.

is given by ref 30. The results of applying this to copper are given below. This expression has been generalized for binary metal oxides, but agreement with experiment in this case requires *ad hoc* expressions for the mass dependence which are still being investigated.

In many cases where strongly covalent bonding occurs, Debye theory would not be expected to work. In such cases there is the option of using a single set of atomic displacements, and specifying the important correlations. Further correlations, which are principally a function of interatomic distance, are interpolated, and assumed to tend to zero for outer shells. A variant of this option which is also available is to define the correlations in terms of three refinable polynomial coefficients. This option ensures a realistic model of disorder for both methods, and reduces the number of free parameters when compared to the third method available, which is to refine XRD and EXAFS thermal parameters independently. In the latter case, because only the mean-square displacements relative to the central atom are available, it is necessary to approximate σ_p^2 for multiple scattering by

$$\sigma_p^2 \sum {}^1/_2 n^2 \sigma_{0a}{}^2 \cos^2(\alpha_a/2) \qquad (23)$$

Where the sum is over all unique atoms, and σ_{0a}^2 is the mean-square relative displacement between atom *a* and the central atom (except the case that a is itself the central atom when σ_{10}^2 is used).

Results

Results are presented here for three well-characterized compounds, Cu metal, CuO, and RuO_2, and for the structurally more complex compounds Ba_2InO_3F, $LaCaGaCuO_5$, and $RbGeIO_6$,[5] whose structures have previously been investigated by powder diffraction. The procedure followed in all cases was to obtain an approximate structure using an XRD-only refinement, then perform the combined refinement with $W_{exafs} = W_{xrd} = 0.5$, sometimes using restraints in the initial stages, and then to perform the EXAFS only ($W_{exafs} = 1$) and XRD only ($W_{xrd} = 1$) refinements starting from the result of the combined refinement.

Cu Metal. Face centered cubic copper metal provides a simple test of the program as only one structural parameter, the cell parameter **a**, can be refined. The spectra were fitted using the Debye model to generate disorder parameters, and also with refined XRD and EXAFS disorder terms. When disorder terms were included a total of 21 parameters were refined. These were the following: A1, A2, ... A7, EXAFS Debye−Waller terms ($2\sigma^2$) for the first seven shells; EF, EXAFS edge energy; GAMMA, effective core-hole width and experimental resolution (in eV); MTR1, MTR2, excited and scattering atom muffin-tin radii; BACK0, ... BACK3, XRD background parameters; BH, CH, peak width parameters defined by $W^2 =$ AH $\tan^2\theta +$ BH $\tan\theta +$ CH; MIXB, Lorentian component of the peak profile function defined by $M =$ MIXA + MIXB $\times 2\theta$; OFFSET, XRD zero offset due to sample position; SCALE, XRD amplitude factor; and BI1, isotropic thermal factor.

Attempts to include AH and MIXA (defined above) or the EXAFS amplitude factor AFAC improved the fits only slightly and resulted in strong correlations between parameters and some unphysical values. These values were set to 0, 0, and 0.95, respectively. The EXAFS DW terms for shells higher than 7 were set to 0.035, slightly higher than the maximum refined value. Multiple scattering paths to 14 Å path lengths were included, with single scattering contributions for atoms to 10 Å. A reasonable quality of fit to both spectra was obtained using the weighting scheme $W_{exafs} = W_{xrd} = 0.5$, giving agreement with known cell parameters to within about 0.001 Å.

Table 1. Principal Parameters for Fits to Cu Foil[a]

	$W_{exafs} = W_{xrd} = 0.5$	$W_{exafs} = 1$	$W_{xrd} = 1$	neutron/D[31]
a/Å	3.616(000)	3.612(004)	3.616(000)	3.6148
B_{iso}/Å^2 (Cu)	0.15(10)		0.07(09)	0.56
A1 (Cu)	0.016(000)	0.016(001)		0.017
A2 (Cu)	0.028(008)	0.028(009)		
A3 (Cu)	0.022(002)	0.022(003)		
A4 (Cu)	0.019(002)	0.019(003)		
A5 (Cu)	0.025(008)	0.025(011)		
A6 (Cu)	0.026(033)	0.026(037)		
A7 (Cu)	0.023(006)	0.022(007)		
R_{exafs}	21.28	21.11		
R_{wp}	32.31		32.28	
P	22	12	11	

[a] Column 1: combined refinement with $W_{exafs} = W_{xrd} = 0.5$. Column 2: EXAFS refinement. Column 3: XRD refinement. 2σ statistical errors are given for parameters actually refined. Parameters are defined in the text (Results, Cu Metal).

The principal parameters are shown in Table 1 together with 2σ statistical errors, *R* factors, and the number of refined parameters *p*. The fits are shown in Figures 1a and 1b. The EXAFS and XRD spectra were also refined independently (using $W_{exafs} = 1$ then $W_{xrd} = 1$). The improvement in fit was very small in each case demonstrating that the combined analysis using a single coordinate description can provide good quality fits simultaneously. Refined values of **a** were rather smaller for the EXAFS case. It is noteworthy that for the EXAFS method the statistical errors for **a** are about 50 times those for the XRD method. In such a case it would be expected that the combined method would give a less reliable cell parameter than XRD data alone. Although EXAFS DW factors are subject to systematic errors, for example due to background subtraction, the technique gives much smaller relative errors than XRD and can provide more accurate information on thermal or static disorder.

For these spectra both the correlations and the $\langle u^2 \rangle$ values were also calculated by Debye theory.[30] The neutron Debye temperature of copper at 298 K was used, taking θ_D to be 317 K, an average of literature values,[31,32] rather than using the ideal zero temperature value of 343 K as previously.[10] These values gave reasonable fits for the EXAFS, with R_{exafs} of 26.5, with slightly different values for the muffin-tin radii and γ. If AFAC is also refined, the fit is better still, $R_{exafs} = 24.3$, but AFAC values of greater than unity are required. Previously[9] the refined value of AFAC was 0.85. Here the calculations differ not only in the new value of θ_D and treatment of disorder but also in the use of an X_{alpha} (with $\alpha = {}^2/_3$) rather than a von Barth and Hedin ground state term in the exchange. Such potentials give consistently higher values of AFAC than previously. Although they would appear to be less successful in giving the correct amplitudes, the overall fit is considerably better. Most of the lack of fit using the Debye model was associated with peaks with a large multiple scattering contribution which probably reflects an inadequacy in the treatment of multiple scattering disorder.

(30) Beni, G.; Platzman, P. M. *Phys. Rev. B* **1976**, *14*, 1514. Bohmer, W.; Rabe, P. *J. Phys. C* **1979**, *12*, 2465.

(31) Flinn, P. A.; McManus, G. M.; Rayne, J. A. *Phys. Rev.* **1961**, *123*, 809. De Wames, R. E.; Wolfram, T.; Lehman, G. W. *Phys. Rev.* **1963**, *131*, 528−529.

(32) Nilsson, G.; Rolandson, S. *Phys. Rev. B* **1993**, *7*, 2393.

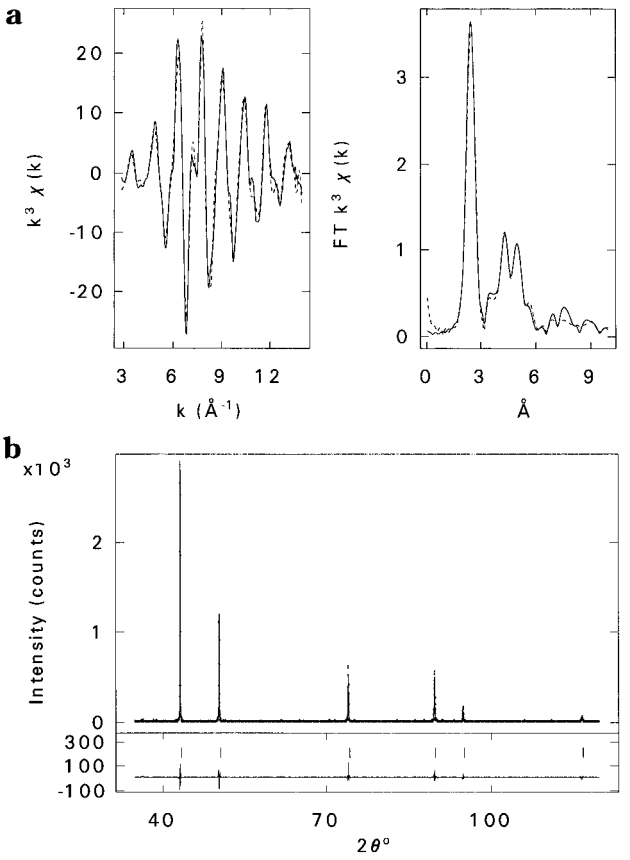

Figure 1. (a) EXAFS fits to the Cu K edge of Cu foil showing experiment (solid) and theory (dotted). The k^3 weighted EXAFS is shown in the left-hand frame. The right-hand frame shows the corresponding Fourier transform, which includes the effect of the central and first shell scattering atom phase shift. (b) Profile fit to the powder diffraction data from Cu foil. Dots are observed intensities, the upper continuous line the calculated profile, and the lower continuous line the difference. Tick marks show the reflection positions.

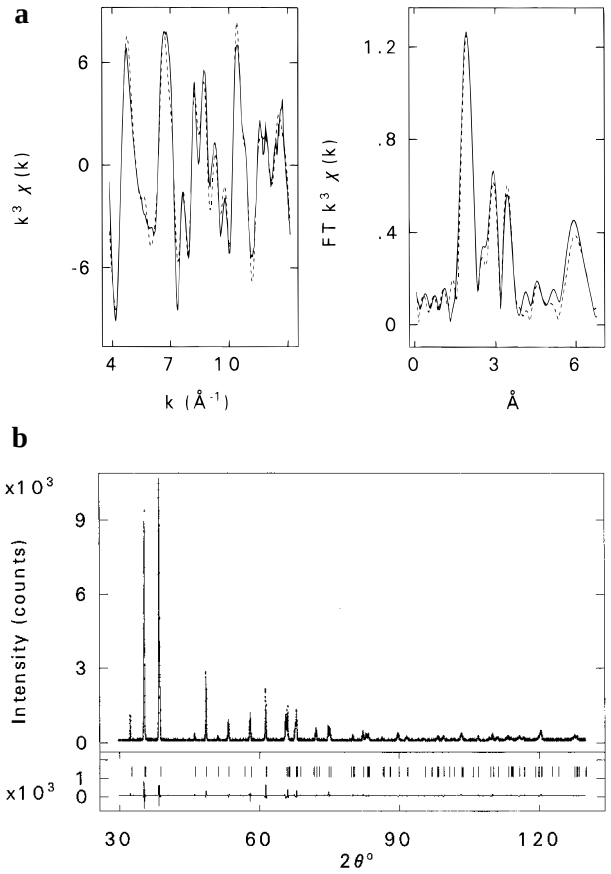

Figure 2. (a) EXAFS fits to the Cu K edge of the CuO. Details as for Figure 1a. (b) Profile fit to the powder diffraction data from CuO. Details are for Figure 1b.

The XRD data fitted as well as with a refined B_{iso} only if the monochromator coefficient (Cu Kα_1 from a quartz monochromator was employed) was adjusted from 0.80 to 0.53. The refined value of 0.07(9) was very different from the neutron value of 0.55. Using this value gave an R_{wp} of 32.66 which although not unreasonable is poorer than would be expected. It would appear that EXAFS gives Debye−Waller factors in excellent agreement with neutron values (neutron DW factors are also in very good agreement with calorimetric values[31]) but there appear to be systematic errors in the XRD method in addition to the large uncertainties derived from the fact that few diffraction peaks occur in the data range. These problems in powder diffraction determined temperature factors, which are strongly correlated with the monochromator coefficient, are well-documented and result from problems in fitting background and the peak profile edges.

CuO. CuO is monoclinic, with space group *C*2/*c* and one adjustable positional parameter—the oxygen *y*-coordinate. The structure was fitted to 6.8 Å resulting in 62 shells; 2968 MS paths were included. Structure was present beyond this limit but was ignored. An EXAFS *R* factor of 21.9% signified a moderately good fit; most of the lack of fit was associated with peaks with a substantial MS contribution which again probably results from the treatment of the disorder. The XRD R_{wp} of 14.6% was almost identical to a refinement in which the EXAFS data were excluded. The structural parameters obtained together with literature values[33] are shown in Table 2. We note that although the small differences in cell parameters between the XRD and single-crystal results are probably due to systematic errors in our diffraction measurements, CuO may be slightly non-stoichiometric and oxygen deficiencies will affect the results. Refinement of the EXAFS data alone, starting from the values obtained in the combined refinement, showed almost no movement. This is probably due in part to lack of convergence because of the strong correlations between the cell parameters. It would be anticipated that slightly improved fits could be obtained with rather different values of the cell parameters. Table 2, as with subsequent tables, also shows the calculated first-shell distances (not refined) and previous single-crystal data.[32] The combined method gives both better agreement with single-crystal data and smaller errors for the oxygen *y*-coordinate when compared to the result using $W_{xrd} = 1$. This suggests that the EXAFS is making some contribution to the analysis even in a case where a Rietveld refinement alone would be expected to be sufficient. As with many metal oxides, the large statistical errors in the isotropic thermal factor of the oxygen reveal that this quantity is poorly defined. In contrast, the first-shell Debye−Waller factors for the EXAFS are well-defined, and provided a suitable model for calculating the correlations is available the technique may offer a better estimate of the effect of disorder than does XRD.

RuO_2. RuO_2 is tetragonal with two molecules per unit cell and has the rutile structure (space group $P4_2/mnm$, No. 136) with ruthenium in the 2a positions (0,0,0) and oxygen in the 4f positions (*x*,*x*,0). The only refinable positional parameter is, therefore, the oxygen *x*-coordinate. The fit to the XRD data is shown in Figure 3b and required the use of a preferred orientation parameter. The EXAFS fit (Figure 3a) suffers from

(33) Asbrink, S.; Lorrby, L. J. *Acta Crystallogr. B* **1982**, *24*, 1968. Asbrink, S.; Lorrby, L. J. *Acta Crystallogr. B* **1970**, *26*, 8.

Table 2. Principal Parameters for Fits to CuO[a]

	$W_{exafs} = W_{xrd} = 0.5$	$W_{exafs} = 1$	$W_{xrd} = 1$	single crystal
a/Å	4.6915(0002)	4.6915(0037)	4.6915(0002)	4.6837(0005)
b/Å	3.4210(0001)	3.4210(0023)	3.4210(0001)	3.4226(0005)
c/Å	5.1333(0002)	5.1333(0011)	5.1334(0002)	5.1288(0006)
β/deg	99.43(0.00)	99.43(0.08)	99.43(0.00)	99.54(0.01)
O *y*	0.4179(0005)	0.4180(0054)	0.4155(0019)	0.4184(0013)
Cu−O/Å	1.9544	1.9543	1.9587	1.9585
Cu−O/Å	1.9611	1.9612	1.9593	1.9628
B_{iso}/Å^2 (Cu)	0.48(0.04)		0.48(0.04)	0.48(0.02)
B_{iso}/Å^2 (O)	0.29(0.16)		0.29(0.14)	0.62(0.09)
A1−2 (O)	0.005(001)	0.005(001)		
A3 (O)	0.010(003)	0.011(005)		
A4−8 (Cu)	0.012(001)	0.012(001)		
A9/11/13−18 (O)	0.014(007)	0.017(014)		
A10 etc. (Cu)	0.018(001)	0.018(002)		
A22 etc. (O)	0.020(009)	0.021(014)		
R_{exafs}	21.88	21.76		
R_{wp}	14.64		14.64	
p	28	16	17	

[a] Column 4: single crystal data.[33] For other details see Table 1.

Table 3. Principal Parameters for Fits to RuO_2[a]

	$W_{exafs} = W_{xrd} = 0.5$	$W_{exafs} = 1$	$W_{xrd} = 1$	single crystal
a/Å	4.4929(0002)	4.4930(0045)	4.4929(0000)	4.4919(0008)
c/Å	3.1068(0001)	3.1068(0038)	3.1068(0001)	3.1066(0006)
O *x*	0.3054(0016)	0.3059(0067)	0.3054(0029)	.3058(0016)
Ru−O/Å	1.9407	1.9436	1.9407	1.9426
Ru−O/Å	1.9853	1.9835	1.9853	1.9836
A1−2 (O)	0.002(001)	0.002(002)		
A3 (Ru)	0.001(001)	0.001(002)		
A4−5 (O)	0.016(017)	0.019(027)		
A6−7 (Ru)	0.003(001)	0.003(001)		
A8−11/14−18 (O)	0.012(008)	0.013(012)		
A12−13 (Ru)	0.005(003)	0.006(003)		
B_{iso}(Ru)/Å^2	0.08(0.14)	0.08(0.13)	0.38(0.01)	
B_{iso}(O)/Å^2	1.19(0.48)	1.19(0.45)	0.52(0.01)	
R_{exafs}	26.86	26.97		
R_{wp}	23.61		23.61	
p	27	13	17	

[a] Column 4: single crystal data.[34] For other details see Table 1.

difficulties in background subtraction, which appears to have inhibited attempts to refine the phase shift parameters. As the spectra again give good agreement with single-crystal data[34] no further attempt to improve the analysis was made. The fit to the XRD data alone was virtually identical to that obtained with the combined fit. The EXAFS-only result gave a slightly different value for the oxygen *x*-coordinate, which was actually in closer agreement with the single-crystal result than the other fits. The error on the combined fit is slightly lower than that in the XRD alone case, and this again therefore represents a case in which the EXAFS may be contributing useful information on the positional coordinate. It is noteworthy that although R_{exafs} for the combined fit is better than that for the EXAFS-only fit, Φ_{exafs} (eq 3) is smaller as expected.

Ba_2InO_3F. This compound has a structure related to that of K_2NiF_4 but with fluoride/oxide ordering, giving rise to the space group *P*4/*nmm* and producing infinite layers formed from linked InO_5 square pyramids separated by BaF layers.[35] The combined refinement gave an good fit to the In K edge EXAFS data, although there were problems with the barium contribution, *vide infra*.

The results in Table 4 show that the combined program gives an improved result relative to those obtained by EXAFS or XRD alone in terms of error values for the majority of refined parameters. However, inspection of the values shows that significant errors and high temperature factors are attached to the fluoride ion position. The EXAFS analysis carried out alone generates a fluorine position which has a very large error associated with it probably showing an ill-defined site; a single light atom such as fluorine contributes little to EXAFS scattering intensity. Also difficulties were encountered in a region of the spectrum around 12 Å^{-1}, due to an artifact in the data, which particularly affected refinement of the barium contribution. This is probably the cause of a relatively high error in the Debye−Waller term for barium in shells 9 and 11 where a maximum value constraint of 0.03 was used. The XRD data analysis also has problems in defining the fluoride ion position; again this is due to poor scattering from this ion and it is noteworthy that it occurs in layers with the strongly scattering barium.

Hence even in the combined refinement the definition of the fluoride ion position remains problematical as neither of the

(34) Boman, C. E. *Acta Chem. Scand.* **1970**, *24*, 116.
(35) Needs, R. L.; Weller, M. T. *J. Chem. Soc. Chem. Commun.* **1995**, 353. Baltz, D.; Plieth, K. *Z. Elektrochem.* **1955**, *59*, 545.

Table 4. Principal Parameters for Fits to Ba_2InO_2F[a]

	$W_{exafs} = W_{xrd} = 0.5$	$W_{exafs} = 1$	$W_{xrd} = 1$	neutron
a/Å	4.1635(0001)	4.1635(0111)	4.1635(0001)	4.1641(0002)
c/Å	13.9501(0005)	13.9501(0967)	13.9503(0004)	13.9439(0008)
O1 *z*	0.2529(0009)	0.2529(0073)	0.2507(0037)	0.2507(0008)
F *z*	0.4205(0025)	0.4205(0095)	0.4200(0049)	0.4275(0002)
O2 *z*	0.0852(0012)	0.0852(0046)	0.0849(0051)	0.0824(0001)
Ba1 *z*	0.3811(0004)	0.3811(0038)	0.3819(0004)	0.3808(0001)
Ba2 *z*	0.1015(0004)	0.1015(0036)	0.1033(0004)	0.1028(0001)
In *z*	0.2359(0005)	0.2359(0017)	0.2338(0005)	0.2325(0001)
In−O/Å	2.0951	2.0951	2.0769	2.092
In−O/Å	2.1026	2.1026	2.0951	2.110
In−F/Å	2.5744	2.5744	2.5970	2.719
A1−2 (O)	0.007(0.001)	0.007(0.002)		
A3 (F)	0.027(0.014)	0.027(0.029)		
A4−5 (Ba)	0.016(0.002)	0.016(0.006)		
A6 (In)	0.014(0.002)	0.014(0.005)		
A9/11 (Ba)	0.030(0.000)	0.030(0.025)		
A14 etc. (In)	0.014(0.002)	0.014(0.005)		
B_{iso}(O1)/Å^2	1.25(0.89)		1.61(0.88)	1.15(3)
B_{iso}(F)/Å^2	1.87(1.58)		1.56(1.55)	2.67(6)
B_{iso}(O2)/Å^2	2.71(1.88)		2.17(1.77)	1.48(4)
B_{iso}(Ba1)/Å^2	0.54(0.18)		0.51(0.17)	0.96(4)
B_{iso}(Ba2)/Å^2	0.58(0.19)		0.45(0.18)	0.92(4)
B_{iso}(In)/Å^2	0.55(0.16)		0.03(0.17)	0.53(3)
R_{exafs}	19.96	19.67		
R_{wp}	11.67		11.61	
R_{neut}				1.47
p	38	22	24	43

[a] Column 3: previous data.[35] Column 4: neutron diffraction data. For other details see Table 1.

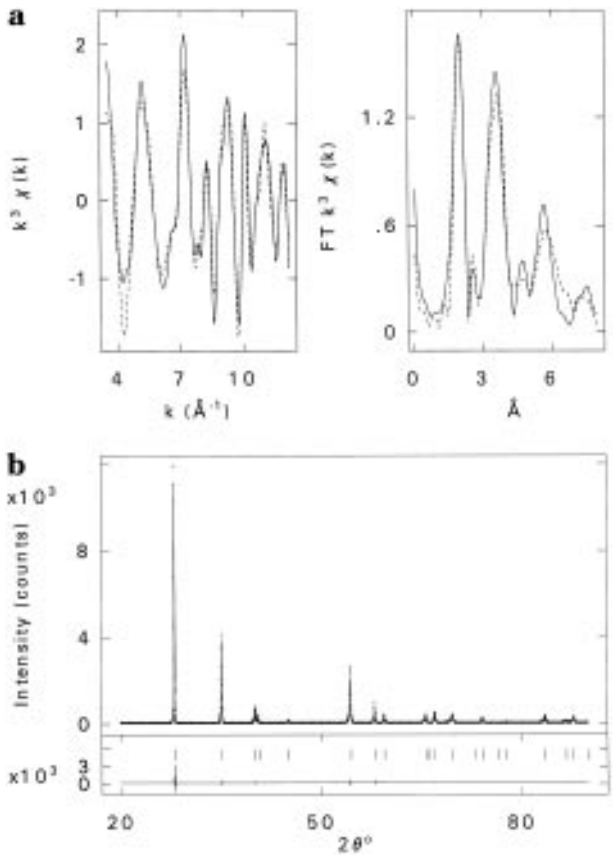

Figure 3. (a) EXAFS fits to the Ru K edge of RuO_2. Details as for Figure 1a. (b) Profile fit to the powder diffraction data from RuO_2. Details as for Figure 1b.

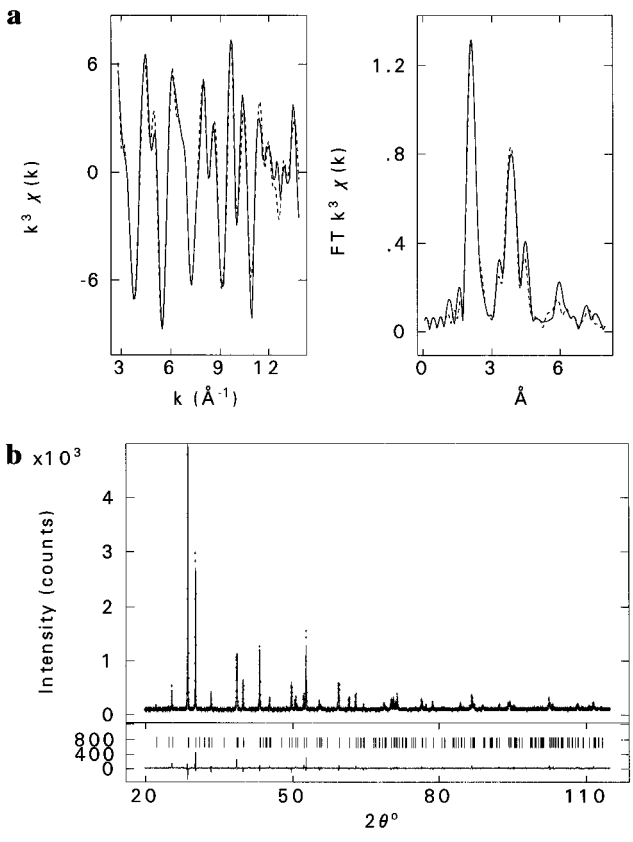

Figure 4. (a) EXAFS fits to the In K edge of Ba_2InO_3F. Details as for Figure 1a. (b) Profile fit to the powder diffraction data from Ba_2InO_3F. Details as for Figure 1b.

contributing data sets are able to define it accurately. A powder neutron diffraction analysis however does provide a better definition of the fluoride ion position due to the relatively high fluorine scattering length for neutrons, Table 4. The fluorine ion position is significantly different from that obtained from EXAFS and XRD and the errors on the *z*-coordinate fall by a factor of 10.

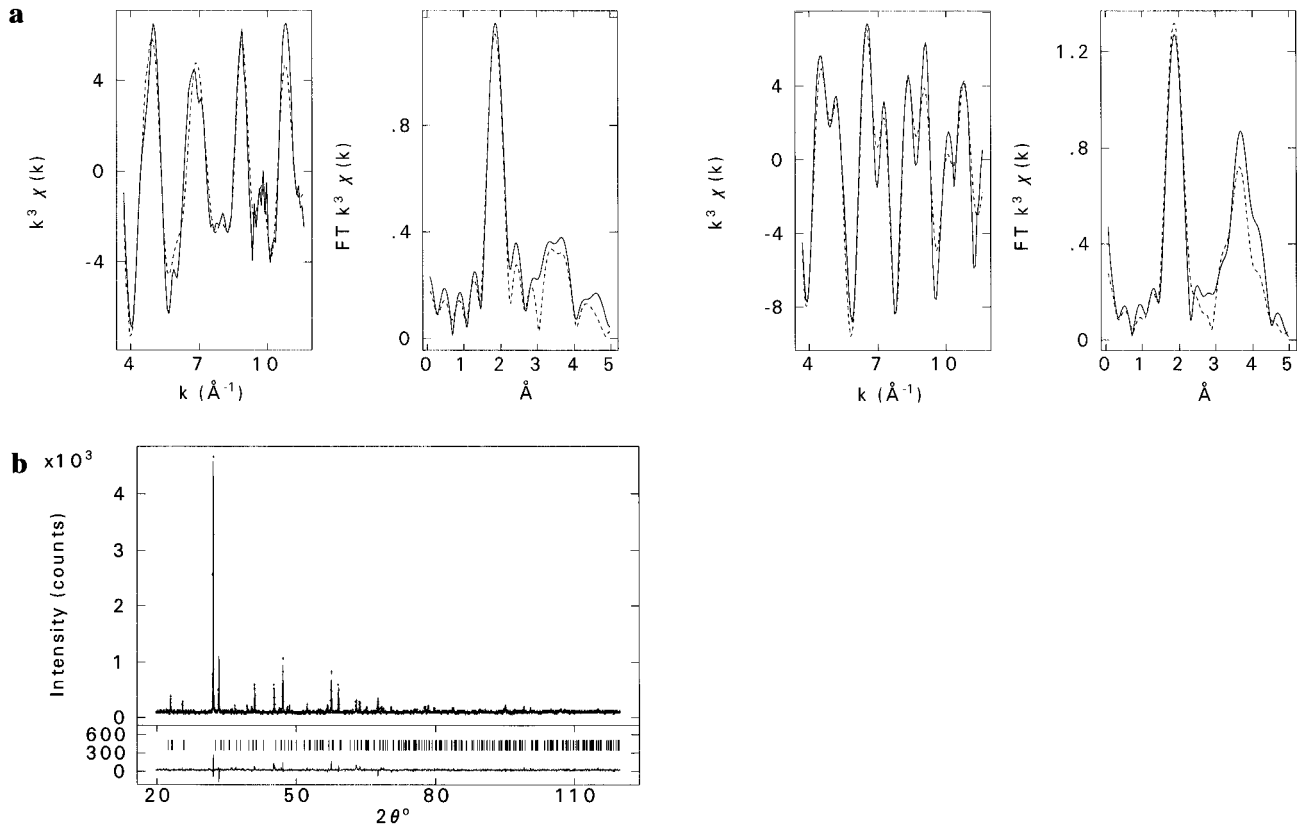

Figure 5. (a) EXAFS fits to the Cu K edge (left) and Ga K edge (right) of $La_{0.9}Ca_{1.1}GaCuO_5$. Details as for Figure 1a. (b) Profile fit to the powder diffraction data from $La_{0.9}Ca_{1.1}GaCuO_5$. Details as for Figure 1b.

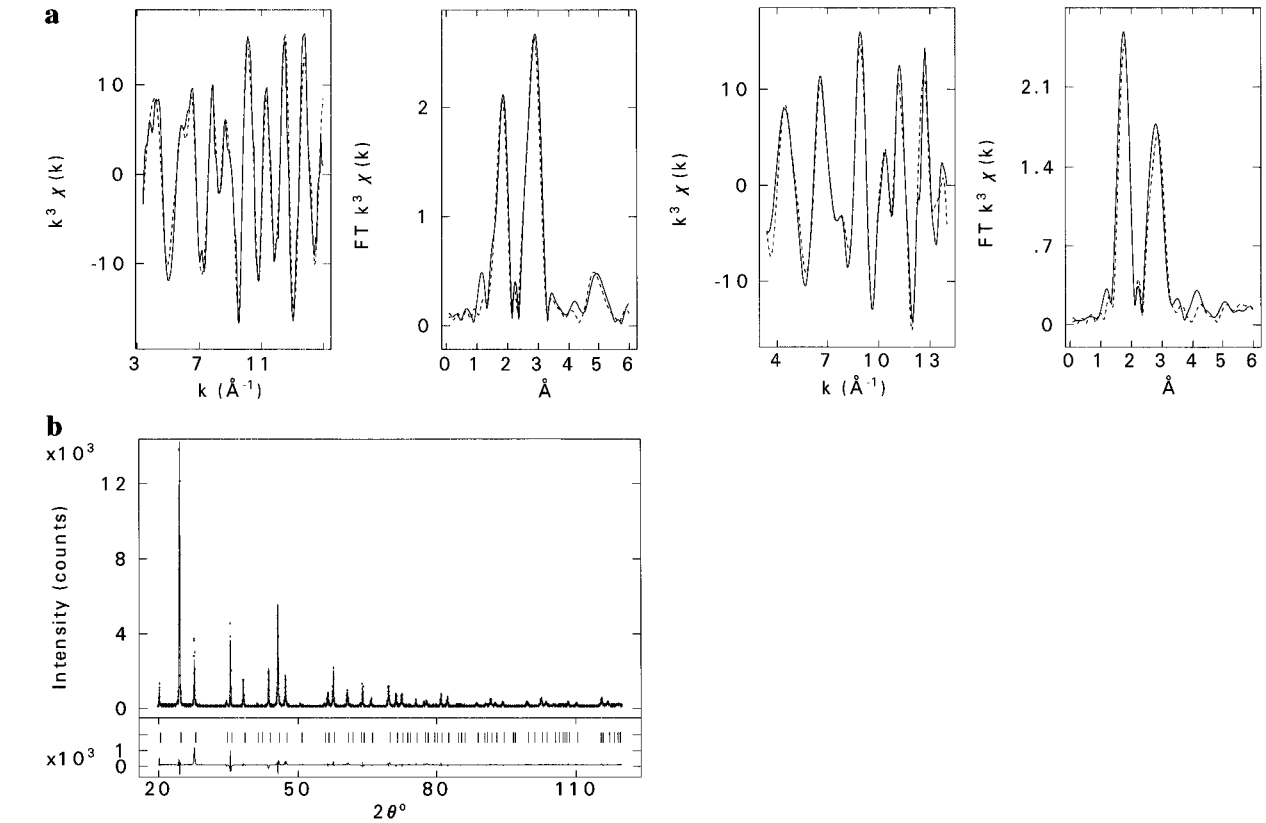

Figure 6. (a) EXAFS fits to the Ge K edge (left) and 1 K edge (right) of $RbGeIO_6$. Details as for Figure 1a. (b) Profile fit to the powder diffraction data from $RbGeIO_6$. Details as for Figure 1b.

Despite an overall improved result using the combined program as opposed to EXAFS/XRD alone, the values obtained are not as accurate as those gained from neutron data. Ideally, refinement of single-crystal data would be undertaken; however, in the absence of such data, this system would clearly benefit from combined neutron and EXAFS data refinement. The capacity for simultaneous refinement of powder neutron diffraction and EXAFS has recently been incorporated in the program, although work on including time-of-flight data is still in progress.

Table 5. Principal Parameters for Fits to $LaCaGaCuO_{5-x}$ with La:Ca 0.9:1.1[a]

	$W_{exafs} = W_{xrd} = 0.5$	$W_{exafs} = 1$	$W_{xrd} = 1$	single crystal (LaCa(1:1))
a/Å	15.9047(0010)	15.9047(9750)	15.9053(0008)	15.8467(0009)
b/Å	5.5103(0003)	5.5118(5890)	5.5104(0003)	5.5077(0003)
c/Å	5.3204(0003)	5.3217(5929)	5.3205(0002)	5.3188(0003)
O1 *x*	0.9990(0041)	1.0000(0408)	0.9937(0035)	0.9913(0003)
O1 *y*	0.2597(0129)	0.2594(0480)	0.2713(0146)	0.2490(0030)
O1 *z*	0.2542(0143)	0.2549(0531)	0.2413(0141)	0.2520(0020)
O2 *x*	0.1495(0023)	0.1494(0058)	0.1478(0027)	0.1496(0004)
O2 *y*	0.0812(0087)	0.0814(0548)	0.0838(0092)	0.0680(0010)
O2 *z*	0.0364(0117)	0.0363(0833)	0.0536(0081)	0.0330(0020)
O3 *y*	0.6319(0054)	0.6319(0289)	0.6349(0151)	0.6230(0020)
O3 *z*	0.1221(0070)	0.1218(0622)	0.1348(0132)	0.1090(0020)
La/Ca *x*	0.1080(0004)	0.1083(0083)	0.1073(0004)	0.1068(0000)
LaCa *y*	0.0169(0019)	0.0169(0247)	0.0167(0016)	0.0174(0001)
Ga *y*	0.9345(0027)	0.9359(0176)	0.9305(0026)	0.9340(0002)
Ga *z*	0.9662(0059)	0.9665(0399)	0.9625(0047)	0.9611(0004)
Cu *z*	0.0146(0069)	0.0146(0272)	0.0143(0057)	0.0002(0005)
Cu−O1/Å	1.9165	1.9153	1.9247	1.9164
Cu−O1/Å	1.9166	1.9182	1.9253	1.9219
Cu−O2/Å	2.4224	2.4213	2.4048	2.4064
Ga−O2/Å	1.8298	1.8274	1.7806	1.7951
Ga−O3/Å	1.8623	1.8684	1.8691	1.8849
Ga−O3/Å	1.8669	1.8719	1.8949	1.8989
A1/2 (Cu−O1)	0.008(0.001)	0.008(0.002)		
A3 (Cu−O2)	0.030(0.023)	0.031(0.031)		
A4−7 (Cu−La/Ca)	0.030(0.013)	0.031(0.048)		
A8−9 (Cu−Cu)	0.019(0.004)	0.019(0.008)		
A10 (Cu−Ga)	0.032(0.060)	0.034(0.130)		
A22 (Ga−O2)	0.033(0.023)	0.035(0.050)		
A23/24 (Ga−O3)	0.003(0.006)	0.003(0.009)		
A25/26 (Ga−Ga)	0.012(0.006)	0.012(0.008)		
A27 etc. (Ga−La/Ca)	0.031(0.020)	0.032(0.053)		
A35 (Ga−Cu)	0.025(0.039)	0.025(0.069)		
A38 (Ga−Ga)	0.032(0.054)	0.034(0.062)		
B_{iso}(O1−3)/Å^2	0.12(0.77)		0.02(0.82)	0.6(1)/1.7(2)/0.9(2)
B_{iso}(La/Ca)/Å^2	0.00(0.19)		0.55(0.18)	0.94(0.01)
B_{iso}(Ga)/Å^2	0.66(0.53)		0.45(0.41)	0.74(0.03)
B_{iso}(Cu)/Å^2	0.39(0.36)		0.15(0.30)	0.62(0.03)
R_{exafs}	22.28	22.25		
R_{wp}	12.86		12.64	
p	50	35	30	

[a] Column 4: single crystal data[36] for La:Ca = 1:1. For other details see Table 1.

$CaLaGaCuO_{5-x}$. This compound consists of alternate layers of CuO_6 octahedra and GaO_4 tetrahedra coordinated by the larger cations. In the sample actually studied the La:Ca ratio was 55:45, which might be expected to give rise to either oxygen deficiencies or substitution of some Cu^{3+} for Cu^{2+}. The modeling of these effects has not yet been attempted; they were ignored for the XRD fit, and for EXAFS it was assumed that the O3 site was 90% occupied. Both the Cu and Ga K edge EXAFS data were available.

Convergence of these refinements was very slow unless the constraint that the first two distances about the copper site and the second two about the gallim site were equivalent was applied until close to the minimum. Departure from these positions after removal of constraints was very small.

A fit using the Cu edge alone (to a higher maximum *k* value than with the combined data) gave an EXAFS *R* factor of around 19%—better than using both edges. This is due to the limited *k*-range and poorer quality of the Ga edge data that were obtained, and consequent uncertainties in the background subtraction. The overall result, with an *R* factor of 23%, is however acceptable, and the coordinates obtained are not significantly different from those using the Cu edge only.

The single-crystal data[36] with which our results are compared (Table 5) are for the 1:1 compound and therefore show some small systematic differences from our results. The successful fit to two EXAFS edges and the powder X-ray data indicates that this joint analysis technique will prove powerful where EXAFS data from several edges are available. It is intended that further EXAFS data from the La (L-III) and Ca (K) edges will be collected in the near future and that they will be incorporated into this refinement.

$RbGeIO_6$. The previously published spectra[5] were re-analyzed using the new program. In this case both the Ge and I K edge spectra were used. As the core-hole lifetimes for the two edges are very different[37] it was necessary to introduce an additional variable to account for this. This was achieved by an approximate correction to the imaginary part of the phase shifts given by

$$\Delta F(\delta_l) = 2I\nu_n \frac{\mathrm{d}R(\delta_l)}{\mathrm{d}E} \qquad (24)$$

where $R(\delta_l)$ is the real part of the scattering phase shift. A correction to the imaginary part of the potential $I\upsilon$ was introduced for each spectrum *n*. This allows the same scattering atom phase shifts, calculated assuming an intermediate core hole

(36) Luzikova, A. V.; Kharlanov, A. L.; Antipov, E. V. *Z. Anorg. Allg. Chem.* **1994**, *620*, 326.
(37) Keski-Rahkonen, O.; Krause, M. O. *At. Data Nucl. Data Tables* **1974**, *14*, 140.

Table 6. Principal Parameters for Fits to $RbGeIO_6$[a]

	$W_{exafs} = W_{xrd} = 0.5$	$W_{exafs} = 1$	$W_{xrd} = 1$	previous (XRD/EXAFS)
a/Å	5.0213(0001)	5.0233(0064)	5.0213(0001)	5.0220(0020)
c/Å	6.3784(0003)	6.3849(0771)	6.3784(0003)	6.3760(0020)
O *x*	0.6411(0031)	0.6426(0114)	0.6272(0050)	0.6340(0030)
O *y*	0.0018(0010)	0.0018(0008)	0.0018(0049)	0.0090(0030)
O *z*	0.3474(0017)	0.3463(0071)	0.3625(0023)	0.3670(0010)
Ge−O/Å	1.8888	1.8961	1.8154	1.82/1.900
Ge−I/Å	2.8991	2.9002	2.8991	2.90
I−O/Å	1.8766	1.8839	1.8025	1.78/1.867
A1 (Ge−O)	0.008(0.001)	0.008(0.002)		
A2 (Ge−I)	0.005(0.001)	0.006(0.001)		
A3 etc. (Ge−O)	0.053(0.008)	0.048(0.014)		
A4 (Ge−Rb)	0.034(0.007)	0.034(0.010)		
A7 (Ge−Ge)	0.012(0.003)	0.012(0.003)		
A9 (Ge−I)	0.032(0.022)	0.029(0.033)		
A12 (I−O)	0.002(0.001)	0.003(0.001)		
A13 (I−Ge)	0.004(0.001)	0.005(0.001)		
A14 etc. (I−O)	0.017(0.012)	0.025(0.027)		
A15 (I−Rb)	0.029(0.014)	0.028(0.017)		
A18 etc. (I−I)	0.018(0.007)	0.019(0.010)		
A20 (Ge−O)	0.003(0.004)	0.004(0.005)		
B_{iso}(O)/Å^2	0.62(0.46)		0.47(0.41)	0.60
B_{iso}(I)/Å^2	0.23(0.13)		0.28(0.12)	0.23
B_{iso}(Ge)/Å^2	0.24(0.25)		0.20(0.23)	0.24
B_{iso}(Rb)/Å^2	1.44(0.16)		1.49(0.15)	1.43
R_{exafs}	22.36	21.66		
R_{wp}	17.62		17.05	
p	41	27	19	

[a] Column 4: previous results from ref 10. Nomenclature for A shows edge element (Ge or I) and shell atom type.

lifetime to be used for both spectra, although the excited central atom will of course be unique to each spectrum.

The metal atoms occupy special positions in the space group *P*312 so only the oxygen (in general positions 6*l*) can be refined. The refinement yielded a new oxygen coordinate (Table 6) which differs substantially from that obtained from the XRD spectra alone. This confirms that the Ge−O distance (1.889(1) Å) is slightly longer than the I−O distance (1.878(1) Å) which is in agreement with the previous EXAFS values of 1.90 and 1.87 Å, respectively. This result should be compared with an XRD only refinement where the position of the oxygen atom is poorly defined leading to incorrect metal oxygen distances of 1.82 and 1.78 Å.

The combined refinement gave an R_{wp} of 17.7% compared to a value for XRD alone of 17.0%. The overall EXAFS *R* factor in this refinement of 22.4% was comparable with the previous values of 23.9% and 21.3% for the individual EXAFS refinements but the data range used here does not extend to quite such low energy as used previously.

Discussion

The results show that an acceptable fit can be obtained to both XRD and EXAFS data using a single structural model. Systematic errors in EXAFS distances can be accommodated by allowing one or more phase shift parameters to be refined. The EXAFS fit is, however, not normally as good as when many individual shell distances are allowed to vary. Normally the quality of the fit to the XRD data is only slightly affected by the constraints introduced by the EXAFS data but the positional parameters of some light atoms may be substantially changed.

Our results suggest discrepancies between the isotropic thermal factors and well-established neutron values for XRD analysis and that EXAFS is far more suited to obtaining meaningful results on disorder.

In most cases considered here there is some advantage in using the combined method, and in some a very considerable improvement in oxygen positions is obtained. In most cases, however, neutron data are potentially superior to the combined EXAFS/XRD method, yielding results almost as accurate as for single-crystal determinations. In other cases, for example where minor elements or site-mixing are involved, a combined powder-diffraction (ideally neutron) and EXAFS approach will be the best method. A field of particular interest to us is the study of local ordering in AlSi, GaSi, and AlGaSi sodalites, where XRD sees the long-range (disordered) structure and EXAFS the short-range (ordered) structure.

Acknowledgment. We thank Drs. D. B. Currie, W. Levason, R. J. Oldroyd, and G. Sankar for providing data and previous analysis, and to EPSRC for funding. The AWRE Harwell routine VA05A is used under license to one of the authors.

JA953251U